

# On the Relationship between SST Gradients, Boundary Layer Winds, and Convergence over the Tropical Oceans

LARISSA E. BACK

*Department of Earth, Atmospheric and Planetary Sciences, Massachusetts Institute of Technology, Cambridge, Massachusetts*

CHRISTOPHER S. BRETHERTON

*Department of Atmospheric Sciences, University of Washington, Seattle, Washington*

(Manuscript received 20 December 2007, in final form 30 December 2008)

## ABSTRACT

A linear mixed layer model that skillfully reproduces observed surface winds and convergence over the tropical oceans is used to examine the relative influence of boundary layer and free-tropospheric processes on the distribution of climatological surface winds and convergence. The semiempirical model assumes a sub-cloud-layer momentum force balance between pressure gradients, Coriolis acceleration, linearized friction, and downward momentum mixing, and it utilizes boundary conditions from the 40-yr ECMWF Re-Analysis (ERA-40). Observed pressure gradients are linearly decomposed into boundary layer (defined as the region below 850 hPa) and free-tropospheric components, and the surface winds and convergence associated with these components are computed. Results show that surface zonal winds are predominantly associated with a combination of free-tropospheric pressure gradients and downward momentum mixing, whereas the distribution of convergence is primarily due to boundary layer temperature gradients, which are closely related to SST gradients. The authors conclude that the climatological distribution of boundary layer convergence is primarily a function of the pattern of SST gradients and is better regarded as a cause rather than a consequence of deep convection.

## 1. Introduction

Over the tropical oceans, low-level moisture convergence is the dominant source of moisture for precipitation, so one might expect climatological surface convergence to be an important factor determining where climatological deep convection occurs. However, latent heating in deep convective systems can also be viewed as causing upward motion, which must be associated with low-level mass and moisture convergence. This circular relationship explains why surface convergence and deep convection are strongly correlated, but the circular nature of the argument limits our ability to usefully conceptualize the relationship between deep convection and the large-scale circulation, because it

offers no insight into whether surface convergence is a cause or consequence of deep convection.

The motivation of this work is to examine the causal direction of this relationship by studying the relative roles of atmospheric boundary layer (BL) versus deep-tropospheric processes in influencing climatological surface winds and convergence over the tropical oceans, given the observed sea surface temperature (SST) distribution. Although in reality the SST distribution is influenced by the distribution of convection, understanding how the atmosphere responds to the observed SSTs is a critical step in improving our conceptual understanding of the fully coupled ocean–atmosphere system. In this work, we show that surface convergence patterns on seasonal and longer time scales are predominantly determined by the imprint of SST gradients on boundary layer temperature and thereby on surface pressure gradients. This suggests that on climatological scales, dynamically induced low-level convergence resulting from SST gradients can be usefully viewed as a cause of deep convection, as first suggested by Lindzen and Nigam (1987, hereafter LN).

---

*Corresponding author address:* Larissa Back, Department of Earth, Atmospheric and Planetary Sciences, Massachusetts Institute of Technology, Building 54-1624, 77 Massachusetts Avenue, Cambridge, MA 02139.  
E-mail: lback@mit.edu

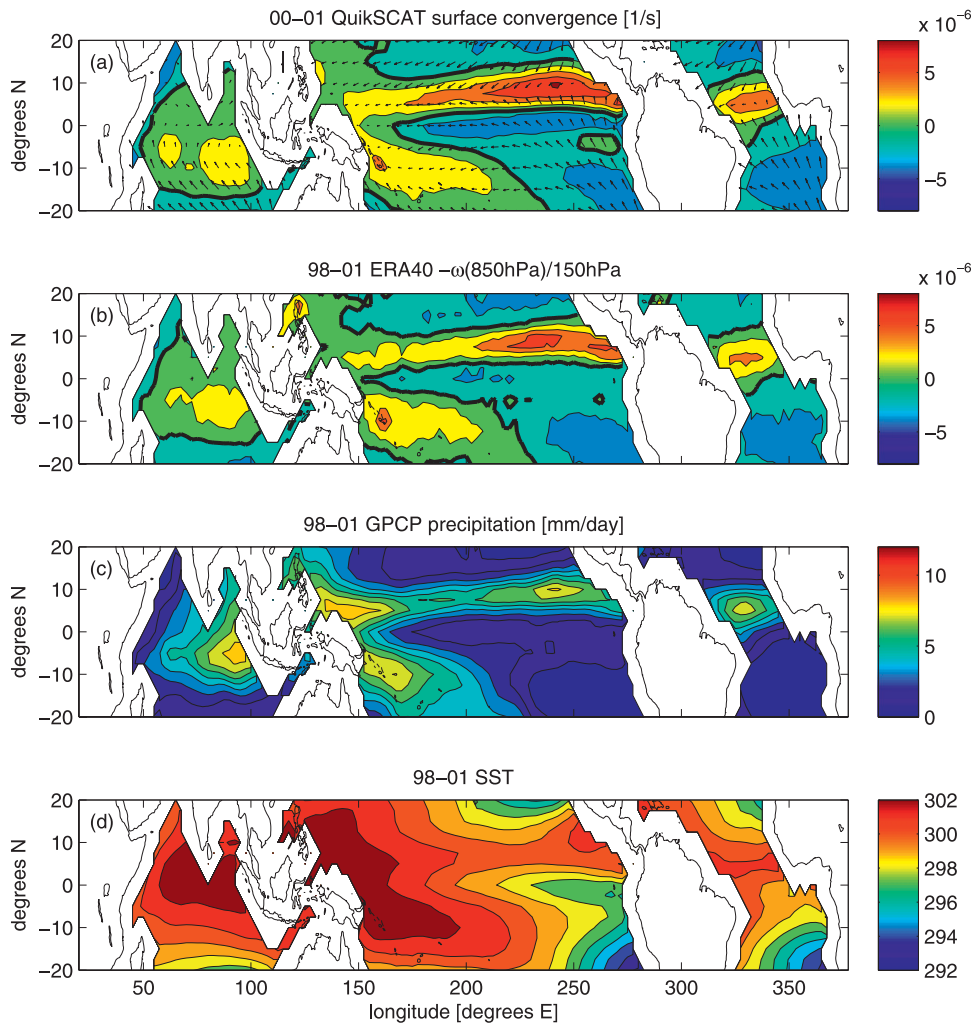


FIG. 1. (a) 2000–01 surface convergence from QuikSCAT with contours of  $2 \times 10^{-6} \text{ s}^{-1}$  (heavy contour shows zero convergence). (b) 1998–2001 ERA-40  $-\omega_{850}/(150 \text{ hPa}) \text{ s}^{-1}$ , representative of mean convergence in the boundary layer, with the same contours as (a). The GPCP 1998–2001 (c) precipitation (contours of  $1 \text{ mm day}^{-1}$ ) and (d) SST (contours of 1 K).

Figure 1 shows the observed climatological relationship between surface convergence, precipitation, and related quantities for illustration purposes [Fu et al. (1994) and others have previously documented similar relationships]. The figure shows the mean 2000–01 vector winds at 10-m height retrieved from the SeaWinds instrument aboard the National Aeronautics and Space Administration (NASA) Quick Scatterometer (QuikSCAT), 850-hPa vertical pressure velocity  $\omega_{850}$  normalized into an approximate equivalent horizontal convergence from the 40-yr European Centre for Medium-Range Weather Forecasts Re-Analysis (ERA-40; Uppala et al. 2005), rainfall from the Global Precipitation Climatology Project (GPCP; Adler et al. 2003), and SST from the ERA-40. Climatological surface conver-

gence and rainfall are strongly correlated, though the relationship is imperfect. Rainfall generally occurs over the warmest SST regions, but rainfall and surface convergence bands tend to be narrower than would be expected from the SST distribution alone. QuikSCAT surface convergence is very well correlated with ERA-40  $\omega_{850}$  ( $20^{\circ}\text{S}$ – $20^{\circ}\text{N}$  annual-mean spatial correlation coefficient  $r = 0.92$ ), suggesting that surface convergence is an excellent proxy for vertical motion near the top of the trade inversion.

The climatological ratio of surface convergence to rainfall varies substantially geographically, as seen in Fig. 1. The region of strongest boundary layer convergence occurs near  $10^{\circ}\text{N}$ ,  $110^{\circ}$ – $140^{\circ}\text{W}$ , where climatological meridional SST gradients are strongest. Surface

wind convergence is also particularly strong over the Atlantic, where meridional SST gradients are large, qualitatively supporting the hypothesis that surface convergence and vertical motion near the trade cumulus inversion are significantly influenced by SST gradients.

The simple but influential LN model takes the view that surface convergence causes deep convection and can in large part be explained by SST gradients. In this idealized model, a significant portion of climatological surface wind and low-level convergence patterns over the tropical oceans is explained as a consequence of SST gradients imprinting on the temperature of the shallow cumulus-capped atmospheric boundary layer, resulting in pressure gradients and frictional convergence.

The extent to which LN's assumptions and choice of constants are physically justifiable has been debated extensively (Neelin 1989; Wang and Li 1993; Battisti et al. 1999; Wu et al. 2000). To obtain a realistic relation between sea level pressure and SST gradients, while also assuming free-tropospheric pressure gradients contribute negligibly to sea level pressure gradients, LN were forced to posit an unrealistically deep SST-influenced boundary layer extending up to 700 hPa. Because they acknowledged the importance of vertical momentum mixing to the zonally averaged Hadley circulation, LN also had to restrict their theory to the zonally asymmetric part of the tropical circulation. Finally, to avoid excessive localization of surface convergence, they were forced to introduce an ad hoc additional back-pressure term.

There is also a more fundamental issue with LN's perspective that surface convergence causes deep convection. Deep convection can play an integral role in determining the tropospheric temperature distribution and the associated large-scale circulations and hence can have a strong influence on surface pressure gradients, winds, and climatological convergence patterns. Although the LN mechanism is plausible, the skill of an LN-type model at reproducing observations does not necessarily imply that surface convergence causes deep convection, because the equations used in LN are to first-order identical to those in a Matsuno–Gill-type model in which surface convergence is a consequence of convective heating (Neelin 1989).

This work tests and expands upon the LN approach by diagnosing observed climatological surface convergence patterns utilizing a linear mixed layer model (MLM; Stevens et al. 2002), which skillfully predicts surface winds and convergence using sea level pressure and 850-hPa horizontal winds, a proxy for winds immediately above the trade cumulus inversion. By forcing this model with atmospheric reanalysis data, we study the relative roles of SST gradients and deep free-tropospheric temperature gradients in forcing surface wind convergence and vertical motion at the height of

the trade cumulus inversion. The model also allows us to interpret the processes LN's back-pressure formulation is standing in for in a more physically consistent manner. We discuss the relationship between the MLM and LN model further in our conclusions.

Relationships between SST, surface convergence, and deep convection have been studied in the past using idealized models of a range of complexities (Zebiak 1982, 1986; Lindzen and Nigam 1987; Neelin 1989; Wang and Li 1993; Chiang et al. 2001; Sobel and Neelin 2006). Models that make the assumption that the latent heating profiles produced by deep convection have a single fixed vertical structure [all of the above models except Sobel and Neelin (2006)] have provided some indication that both SST gradients and deep heating influence surface winds and convergence. Compared to these previous modeling studies, a unique feature of our analysis is the extent to which it is based on observations, as well as the inclusion of the effects of downward momentum mixing on surface winds, which has been shown to have a first-order effect on the surface momentum balance over the oceans (Chiang and Zebiak 2000; Stevens et al. 2002; McGauley et al. 2004).

A motivation for our interest in understanding the extent to which SST gradients influence surface convergence is that recent studies (Trenberth et al. 2000; Zhang et al. 2004; Back and Bretherton 2006) have shown that climatological vertical motion profiles in a 2000-km-wide region of the central-eastern Pacific ITCZ are "bottom heavy" with maximum vertical motion near 850 hPa. These bottom-heavy vertical motion profiles, particularly pronounced in the east-central Pacific ITCZ near 10°N from 120° to 140°W, are associated with latent heating occurring at lower levels than in other deep convective regions and a larger ratio of low-level clouds to near-tropopause cloud (Mote and Frey 2006; Kubar et al. 2007). The amount of bottom heaviness strongly influences the feedback of convection on the column-integrated divergence of heat, moisture, and moist static energy, and thus the large-scale circulation. The east-central Pacific ITCZ is also a region with particularly strong SST gradients and surface convergence. Hence, this may be a region where the LN model is particularly relevant, such that strong SST gradients are driving the convection and affecting the resulting vertical motion profile more in this region than in other tropical rainy regions.

This type of explanation of convective rainfall and heating profile is incomplete because column instability as measured by convective available potential energy (CAPE) seems adequate to support deep convection throughout the tropical ITCZs, and the spectrum of convective cloud depths and the associated vertical

profile of cumulus mass flux must ultimately derive from the local thermodynamic (especially moisture) and shear profiles, which are not predicted by an LN-type model. Nevertheless, it appears to be a useful way to think.

Our observational data are described in section 2. The MLM is described and compared to these observations in section 3. Section 4 uses this model as a framework for interpreting climatological surface winds and convergence as due to a linear combination of SST-induced boundary layer temperature gradients, deep-tropospheric temperature gradients, and downward momentum mixing. In sections 5 and 6, we examine the representation of seasonal cycle variability in the model and compare the mean state to 850-hPa vertical motion in a range of atmospheric general circulation models (AGCMs) forced with climatologically varying SSTs. In section 7, we discuss the implications of these results. This work feeds into a companion paper (Back and Bretherton 2009), in which we develop simple empirical relationships that skillfully predict rainfall and the vertical structure of deep convection based on the surface convergence and the local SST.

## 2. Data description

Monthly averaged 1998–2001 data from ERA-40 were used to provide boundary conditions for the linear boundary layer model and to validate the boundary layer model results. We obtained these  $2.5^\circ \times 2.5^\circ$  gridded pressure-level ERA-40 temperature, wind speed, and geopotential height data, as well as surface-level temperature and pressure data from the Data Support Section of the National Center for Atmospheric Research (NCAR). To examine the robustness of our results to using data from other reanalyses, we also utilize comparable National Centers for Environmental Prediction (NCEP)–NCAR reanalysis data (Kalnay and et al., 1996) and NCEP–Department of Energy (DOE) Atmospheric Modelling Intercomparison Project II (AMIP-II) reanalysis data (NCEP-2; Kanamitsu et al. 2002) from the Climate Diagnostics Center (available online at <http://www.cdc.noaa.gov>).

To provide more accurate surface wind information, we obtained satellite retrievals of surface wind from the NASA SeaWinds instrument on QuikSCAT from Remote Sensing Systems (available online at <http://www.remss.com>). The QuikSCAT surface winds and convergence averaged from 2000 to 2001 from their native  $0.25^\circ \times 0.25^\circ$  grid to the ERA-40 grid are shown in Fig. 1a. In this computation, no attempt was made to correct for sampling errors or biases associated with the diurnal cycle, though rain-flagged pixels were removed. Surface winds from QuikSCAT are one of the quan-

ties assimilated into ERA-40 during this time period, so QuikSCAT and ERA-40 do not provide independent estimates of surface winds. We also used precipitation estimates (1998–2001) from GPCP (Adler et al. 2003), interpolated to the same grid as the ERA-40 data.

In section 6, we compare 850-hPa vertical motion fields and precipitation from four AGCMs forced by seasonally varying sea surface temperatures. These include the NCAR Community Atmosphere Model, version 3 (CAM3); a superparameterized version of the CAM3 (SPCAM); the Geophysical Fluid Dynamics Laboratory (GFDL) Atmospheric Model version 2.12b (AM2.12b); and the NASA Seasonal-to-Interannual Prediction Project version 2 (NSIPP-2) model from the Global Modeling and Assimilation Office (GMAO). Details on these models and simulations can be found in Wyant et al. (2006a,b).

## 3. Linear mixed layer model

We use the steady-state MLM developed by Stevens et al. (2002) to reproduce and explain the observed surface wind distribution over the tropical Pacific. This model assumes the existence of a layer of constant depth  $h$  of vertically uniform wind everywhere over the tropical ocean surface. Over most of the low-latitude oceans, this mixed layer is interpreted as the subcloud layer and cumuli are assumed to flux momentum between the free troposphere and the mixed layer. In coastal stratocumulus regimes, the mixed layer should instead be interpreted as the entire boundary layer with direct entrainment of momentum into the mixed layer by turbulent eddies.

In the MLM, as in observations, the dominant terms in the steady-state BL force balance are the Coriolis acceleration, pressure gradient, Coriolis acceleration, downward momentum mixing, and friction as follows:

$$f\mathbf{k} \times \mathbf{U} + \rho_0^{-1} \nabla P_s = \frac{w_e(\mathbf{U}_T - \mathbf{U})}{h} - \frac{w_d(\mathbf{U})}{h}, \quad (1)$$

where  $f$  is the Coriolis parameter,  $\mathbf{U}$  is the horizontal bulk boundary layer vector wind,  $\rho_0$  is a constant reference density,  $P_s$  is surface pressure,  $w_e$  is an entrainment velocity describing the amount of downward momentum mixing,  $\mathbf{U}_T$  is wind at 850 hPa (the nominal top of the trade cumulus layer), and  $w_d$  is a linearized friction coefficient. Including downward momentum mixing is important to reproducing the observed surface wind distribution (Stevens et al. 2002).

Solving (1) for surface winds yields the following (corrected from Stevens et al. 2002):

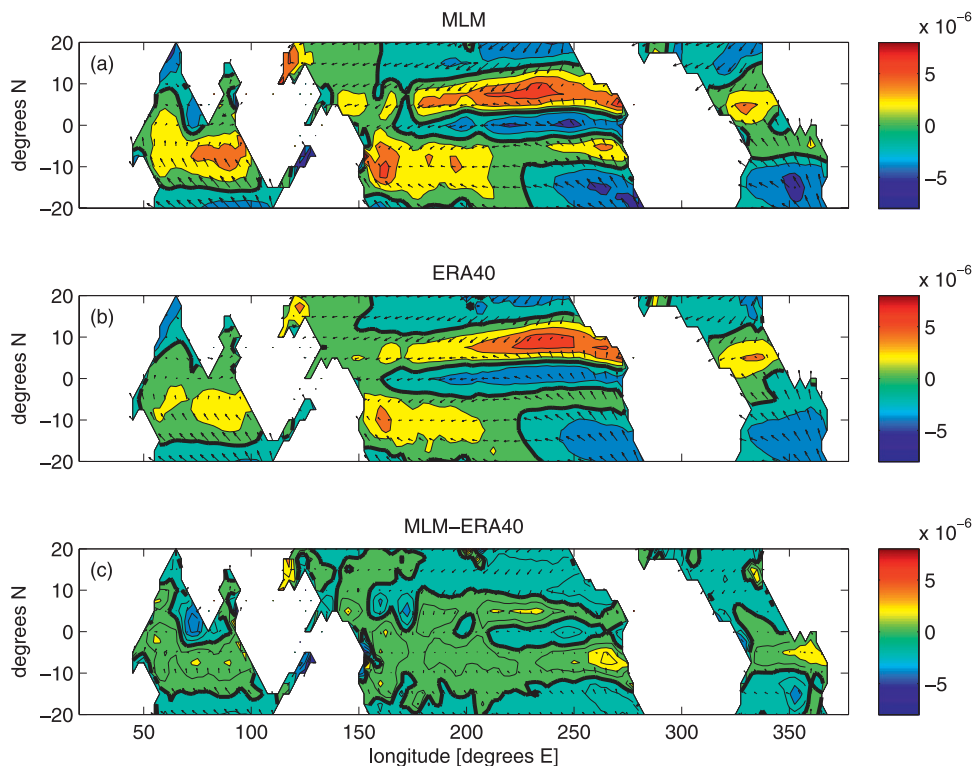


FIG. 2. Annual-mean surface winds and convergence from (a) MLM [ $\mathbf{V}(\partial P_{BL}, U_T, \partial P_i)$ ] forced by ERA-40 and (b) ERA-40, and (c) their difference. Here,  $1^\circ$  arrow length is  $2 \text{ m s}^{-1}$  wind and there are  $2 \times 10^{-6} \text{ s}^{-1}$  convergence contours, except for in (c), where the contour interval is halved and the arrow length is doubled. There is a heavy zero contour for (a)–(c).

$$\begin{aligned}
 U &= \frac{U_T \epsilon_i \epsilon_e + V_T f \epsilon_e - \rho_0^{-1} (f \partial P_s / \partial y + \epsilon_i \partial P_s / \partial x)}{\epsilon_i^2 + f^2}, \\
 V &= \frac{V_T \epsilon_i \epsilon_e - U_T f \epsilon_e + \rho_0^{-1} (f \partial P_s / \partial x - \epsilon_i \partial P_s / \partial y)}{\epsilon_i^2 + f^2},
 \end{aligned} \quad (2)$$

where  $\epsilon_e = w_e/h$  and  $\epsilon_i = (w_e + w_d)/h$ . Stevens et al. (2002) found constant values  $w_e/h = 2 \times 10^{-5} \text{ s}^{-1}$  and  $w_d/h = 1.5 \times 10^{-5} \text{ s}^{-1}$  give a good fit to the Comprehensive Ocean–Atmosphere Data Set (COADS) and NCEP reanalysis data, and we also adopted these values. Our results are fairly insensitive to varying  $\epsilon_e$  and/or  $\epsilon_i$  by a factor of 2, as we show in more detail in the next section.

MLM solutions were calculated from (2) with ERA-40 sea level pressure gradients and 850-hPa horizontal winds as input. Because zonal pressure gradients are small in the tropics, spectral ringing in the ERA-40 output produced noticeable ripples in the derived winds and convergence. These were filtered by applying a three-point zonal running mean to the sea level pressure field and 850-hPa inputs to the MLM.

Figure 2 compares the annual-mean MLM and ERA-40 surface winds and convergence. These should also be

compared with corresponding QuikSCAT observations (Fig. 1). The top two rows and columns of Table 1 give the spatial correlation coefficients of the annual-mean vector winds and convergence with QuikSCAT. For all of the correlation coefficients quantified in Table 1, root-mean-square errors are also given in the bottom half of the table. Because ERA-40 assimilates QuikSCAT winds, ERA-40 annual-mean surface winds are almost perfectly correlated with QuikSCAT, and their convergence fields have a spatial correlation coefficient  $r = 0.99$ . The MLM also has impressive skill at predicting surface vector winds ( $r = 0.98$ ) and convergence ( $r = 0.84$ ) using ERA-40 surface pressure and 850-hPa winds [even more than Stevens et al. (2002) demonstrated using the NCEP reanalysis]. The largest convergence differences between the MLM and ERA-40 are in the eastern Pacific–Southern Hemisphere convergence zone, where the MLM produces too much convergence compared to QuikSCAT, as does ERA-40 to a lesser extent. Interestingly, many of the regions where the MLM produces excess convergence, including the southeastern Pacific and southern Atlantic, correspond to regions where AGCMs tend to produce excess convergence (see section 6 of this work; Biasutti

TABLE 1. Correlation coefficients and RMS error compared with QuikSCAT observations over oceans. Seasonal (DJF, MAM, JJA, and SON) averages and monthly data are anomalies with respect to the simulated time-mean 2000–01 state. The columns titled MLM-BL and MLM-deep correspond to the components of winds and convergence that are associated with gradients of the boundary layer pressure contribution  $\Delta P_{BL}$  and with the combination of 850-hPa pressure gradients and winds, respectively, as in Figs. 4a,b, and the MLM-SST column corresponds to the model version whose mean state is shown in Fig. 5b. MLM-SST BL and SST only correspond to Figs. 5a and 6a, respectively.

	ERA-40	MLM	MLM BL	MLM deep	MLM-SST	MLM-SST BL	MLM-SST SST only
Correlations:							
Mean winds	0.99	0.98	0.83	0.90	0.97	0.76	0.56
Convergence	0.95	0.84	0.85	0.13	0.65	0.62	0.62
Seasonal winds	0.97	0.94	0.77	0.81	0.91	0.65	0.49
Convergence	0.91	0.82	0.78	0.14	0.51	0.48	0.48
Monthly winds	0.89	0.85	0.68	0.72	0.82	0.54	0.40
Convergence	0.76	0.65	0.65	0.12	0.40	0.38	0.38
RMS:							
Mean winds	0.45	0.74	2.43	1.70	0.89	2.66	3.21
Convergence $\times 10^6$	0.74	1.42	1.31	2.51	2.49	2.53	2.53
Seasonal winds	0.40	0.58	0.98	0.88	0.67	1.13	1.30
Convergence $\times 10^{-6}$	0.71	0.98	1.08	1.75	1.72	1.72	1.72
Monthly winds	0.89	1.11	1.35	1.27	1.17	1.54	1.67
Convergence $\times 10^{-6}$	1.42	1.80	1.72	2.28	2.70	2.59	2.59

et al. 2006), which suggests that the reasons for these biases may be worth exploring further.

#### 4. BL-free-troposphere separation

A key assumption made by LN was to specify the sea level pressure field (and surface winds) in terms of only the SST. The MLM is an excellent framework for evaluating this approach, because (2) naturally partitions surface winds and horizontal convergence into contributions from downward momentum mixing and from the free-tropospheric and boundary layer contributions to surface pressure gradients. Following LN, we anticipate the boundary layer contribution to surface pressure gradients will be strongly correlated with local SST gradients. On the other hand, the free-tropospheric pressure gradients and winds (which were only modeled through back pressure in LN) are created by horizontal temperature gradients integrated over the depth of the atmosphere. These reflect the distribution of deep convective heating over the entire tropics, not just the local SST or SST gradients.

For this partitioning, we define the 850-hPa level as the BL top because this is near the climatological trade inversion, which caps active vertical mixing due to turbulence and shallow cumulus convection over much of the tropics. In addition, the 850-hPa surface is convenient because our ERA-40 dataset has been interpolated to pressure surfaces, including 850 hPa, which is close to where bottom-heavy vertical motion profiles peak. Introducing the geopotential  $\Phi$  and denoting a mean over the belt 20°S–20°N by an overline, we write

$$P_s = P_i + \Delta P_{BL} \quad \text{and} \quad (3)$$

$$P_i = 850 \text{ hPa} + \rho_{850}(\Phi_{850} - \bar{\Phi}_{850}). \quad (4)$$

Here,  $P_i$ , which is approximately the pressure at the mean height of the 850-hPa surface, is calculated from zonally smoothed ERA-40 output. The boundary layer contribution  $\Delta P_{BL}$ , calculated as a residual, is proportional to the mean temperature between the surface and 850 hPa.

Figure 3 compares these two contributions to the annual-mean surface pressure patterns, based on ERA-40. Both contributions are important and tend to covary but also differ in important ways. As anticipated by LN,  $\Delta P_{BL}$  is highly correlated with SST. The free-tropospheric pressure contribution  $P_i$  is also loosely correlated with SST (which is why LN were forced to choose an unrealistically deep BL top of 700 hPa) but it is more equatorially symmetric. Over the east Pacific ITCZ, boundary layer thickness variations favor off-equatorial surface convergence whereas the deep-tropospheric pressure gradients favor equatorial convergence. The 850-hPa winds, also shown in Fig. 3c, are predominantly geostrophic.

Figure 4 shows the resulting decomposition of the MLM surface winds and convergence [calculated using (2)] into components resulting from  $\Delta P_{BL}$ ,  $P_i$ , and  $\mathbf{u}_T$ . The majority of the surface zonal wind is associated with 850-hPa winds and pressure gradients. The surface meridional winds, which are associated with most of the convergence, derive mainly from BL pressure gradients. This occurs in part because the two other terms nearly

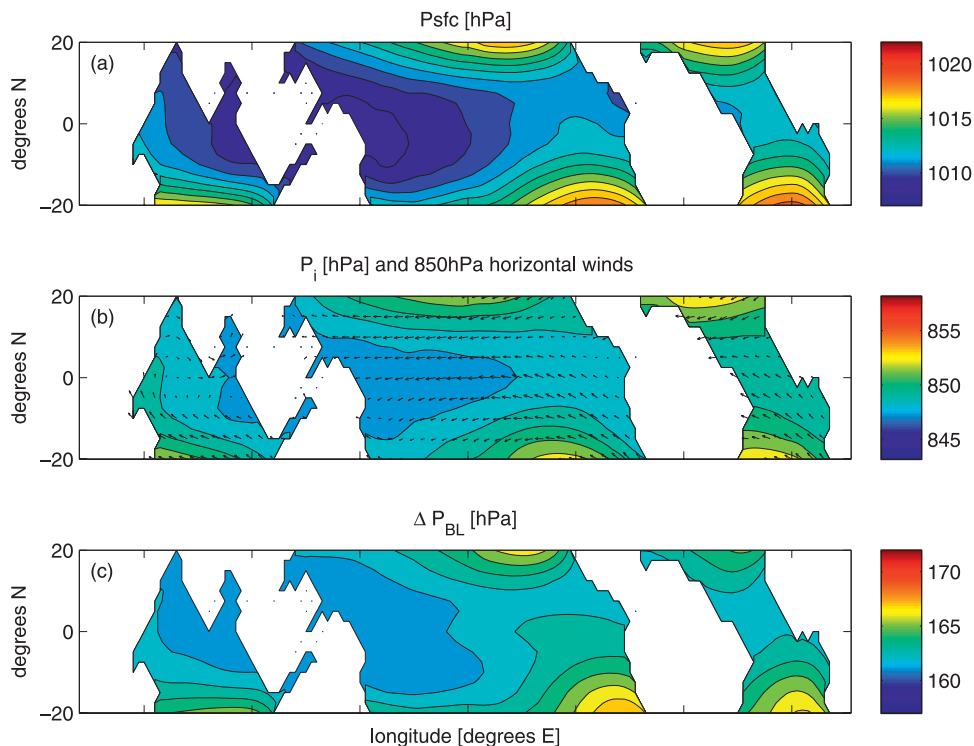


FIG. 3. ERA-40 1998–2001 mean (a) surface pressure, (b) free-tropospheric contribution to surface pressure [ $P_i$  in (4)] and 850-hPa vector winds, and (c) boundary layer contribution to surface pressure from below 850 hPa [ $\Delta P_{BL}$  in (4)]. Here,  $1^\circ$  arrow length is  $2 \text{ m s}^{-1}$  wind.

cancel—the meridional wind and convergence due to downward momentum mixing offset about  $\frac{2}{3}$  of the contribution from deep-tropospheric pressure gradients. This is no coincidence. If one makes the good approximations that the zonal 850-hPa  $U_T$  dominates the 850-hPa meridional wind  $V_T$  and that meridional inversion pressure gradients are larger than zonal pressure gradients, then the meridional, free-tropospheric component of (2) simplifies to

$$V \approx \frac{-U_T f \epsilon_e - \epsilon_i \rho_0^{-1} \partial P_i / \partial y}{\epsilon_i^2 + f^2}.$$

In addition,  $U_T$  is approximately geostrophic, so for our set of parameter choices, the first term in the numerator cancels a fraction  $\rho_0 \epsilon_e / (\rho_i \epsilon_i) \approx 70\%$  of the second term. The extent of this cancellation depends on the choice of coefficients in the MLM, but the general conclusion that surface convergence is mainly due to pressure gradients originating below 850 hPa is quite robust. This conclusion can be quantified in terms of spatial correlation coefficients between the BL and 850-hPa (“deep”) contributions to the annual-mean MLM surface winds and convergence and the corresponding QuikSCAT fields, which are given in the top two rows of the third and fourth columns of Table 1. These correlation coef-

ficients show that both BL and deep contributions to the surface vector winds are important but that the BL contribution is responsible for almost all the skill of the MLM in predicting the surface convergence. The lower half of Table 1 shows the same comparisons using root-mean-square differences in wind and convergence between QuikSCAT and the MLM instead of correlation coefficients; this metric yields similar results.

In Table 2, we examine the sensitivity of our results to the choice of reanalysis product used as a boundary condition and to the doubling or halving of  $\epsilon$ . When NCEP and NCEP-2 are used to provide boundary conditions (top two rows), the MLM is substantially less skillful at reproducing observed winds and convergence: this seems to be due to more noticeable spectral ringing than in ERA-40 (not shown). As in Table 1, the correlation between observations and both BL and 850-hPa contributions to MLM surface winds is substantial. However, the correlations between observed convergence and MLM convergence are largely due to the BL contribution to the MLM. These results are robust to the sizeable range of variations in  $\epsilon$  we examined.

As mentioned in Stevens et al. (2002), the  $\epsilon$  are not strongly constrained by observations, and our choices fall well within the range implied by estimates of  $h$  and  $w_e$ ,

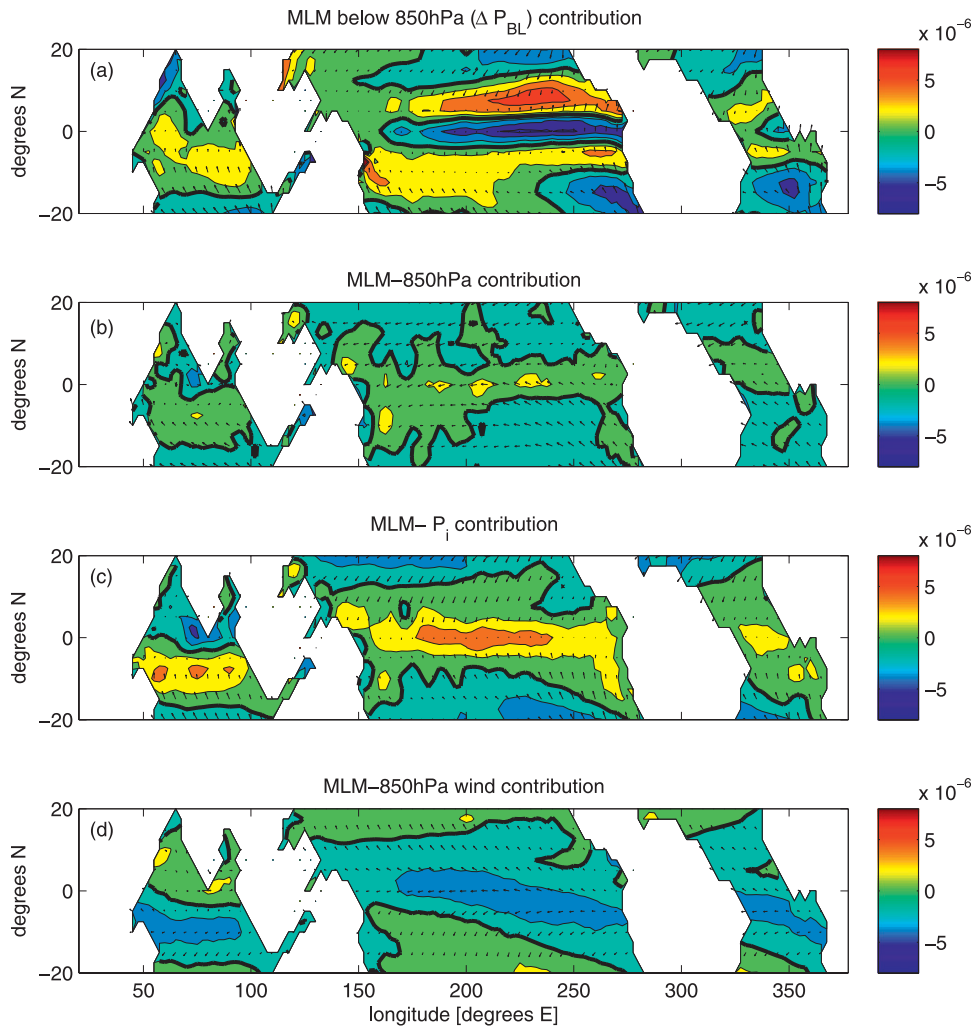


FIG. 4. Components of MLM solution resulting from (a)  $\Delta P_{BL}$ , the boundary layer contribution to surface pressure gradients [ $\mathbf{V}(\partial P_{BL}, U_T = 0, \partial P_i = 0)$ ]; (b) above-850-hPa (free tropospheric) processes [ $\mathbf{V}(\partial P_{BL} = 0, U_T, \partial P_i)$ ]; (c)  $P_i$ , the above-850-hPa contribution to surface pressure gradients [ $\mathbf{V}(\partial P_{BL} = 0, U_T = 0, \partial P_i)$ ]; and (d) downward momentum mixing [ $\mathbf{V}(\partial P_{BL} = 0, U_T, \partial P_i = 0)$ ]. The plotting conventions are the same as Fig. 2. (b) is the sum of (c) and (d).

such as those by McGauley et al. (2004) and de Szoeke et al. (2005) who estimated  $h$  between 500 and 1000 m and  $w_e$  between 1 and 2  $\text{cm s}^{-1}$  using high-resolution data from the Eastern Pacific Investigation of Climate (EPIC2001). This corresponds to  $\epsilon_e$  between  $1e - 5$  and  $4e - 5$ . Other researchers (Ahlgriim and Randall 2006) have estimated  $h$  using data from the Geoscience Laser Altimeter System and then used this estimate combined with moisture and moist static energy budgets using ERA-40 data to diagnose  $w_e$ . Their estimates suggest an average  $h$  around 1200 m and  $w_e$  around 0.5  $\text{cm s}^{-1}$ . However, the momentum mixed layer is less deep than the cloud top in the decoupled and trade cumulus boundary layers that typify most of the subtropical oceans (Holland and Rasmusson 1973).

The result that zonal winds are predominantly due to deep-tropospheric processes but meridional wind and convergence are more strongly influenced by SST gradients is consistent with the AGCM study of Chiang et al. (2001), though their methodology was quite different and focused only on the dominant modes of interannual variability instead of the annual-mean climatology and seasonal cycle as we do. An AGCM study by Bacmeister and Suarez (2002) also corroborates this conclusion about surface zonal winds.

#### Connection to SST

To construct an LN-like model, we must relate gradients in the boundary layer pressure contribution  $\Delta P_{BL}$  to gradients in SST. A simple approximation is to

TABLE 2. The top three rows show the dependence of the correlation coefficients between QuikSCAT and MLM surface wind/convergence (of the mean state) on which reanalysis is used to provide 850-hPa and surface pressure boundary conditions. The remaining rows show sensitivity to the doubling or halving of  $\epsilon$  when using ERA-40 data as boundary conditions.

	MLM	MLM-BL	MLM-deep
NCEP	0.81/0.41	0.66/0.33	0.74/0.16
NCEP-2	0.82/0.64	0.68/0.58	0.76/0.14
ERA-40 control	0.98/0.84	0.83/0.85	0.90/0.13
Doubled $\epsilon_e, \epsilon_i$	0.98/0.83	0.73/0.81	0.90/0.30
Halved $\epsilon_e, \epsilon_i$	0.96/0.75	0.81/0.77	0.87/−0.03
Doubled $\epsilon_e$	0.95/0.79	0.83/0.85	0.80/0.16
Halved $\epsilon_e$	0.95/0.78	0.83/0.85	0.88/0.06
Doubled $\epsilon_i$	0.92/0.76	0.73/0.81	0.89/0.14
Halved $\epsilon_i$	0.92/0.67	0.81/0.77	0.78/0.11

hydrostatically estimate  $\Delta P_{BL}$  by assuming the air temperature varies linearly between a surface value equal to the SST and the ERA-40 850-hPa temperature, which is roughly at the mean inversion height; density can then be linearized about the mean temperature and integrated (as in LN). Figure 5a shows the corresponding MLM estimate of the boundary layer contribution to annual-mean surface winds and convergence patterns. In Fig. 5b, the free-tropospheric contribution (Fig. 4b) to surface winds and convergence has been added to this boundary layer contribution. We refer to the version of the MLM in Fig. 5b as the MLM-SST; its only inputs are SST, ERA-40 850-hPa winds, temperature, and geopotential. The MLM-SST BL-induced convergence field (Fig. 5a) is visually similar and strongly correlated ( $r = 0.76$ ) to that from the regular MLM (shown in Fig. 4a).

As in the MLM, the strongest BL-induced surface convergence in the MLM-SST is found in the central and eastern Pacific ITCZ.

The fifth and sixth columns of Table 1 show the skill of the MLM-SST solution for 2000–01, with and without the contribution from above 850 hPa and measured via a spatial correlation with QuikSCAT, as well as a root-mean-square error. The MLM-SST retains an excellent overall representation of the 2-yr-mean surface winds ( $r = 0.97$ ). Its surface wind convergence has a correlation coefficient of 0.65 with QuikSCAT, which is good but somewhat less skillful than the corresponding value of 0.85 for the regular MLM. As is the case for the MLM, most of the MLM-SST skill in simulating convergence is due to the boundary layer component, whereas including the 850-hPa contribution is important to simulating the surface winds.

Figures 5a,b show that the MLM-SST simulates excess convergence in the Atlantic and Pacific near 10°S. Divergence over the cold tongue is also too strong in the MLM-SST, potentially because of an overestimate of  $\Delta P_{BL}$  resulting from warm air advection from the south and the reduction of turbulent mixing near the surface over cold SST. The increased secondary convergence maximum near the coastline of South America is partially an artifact associated with the strong inversion and subsidence warming capping the stratocumulus clouds in this region. Because of the strong inversion, the average of 850-hPa temperature and SST leads to an underestimate of  $\Delta P_{BL}$  in this region. However, in regions of surface convergence, which are the regions most relevant to deep convection, the MLM-SST shows

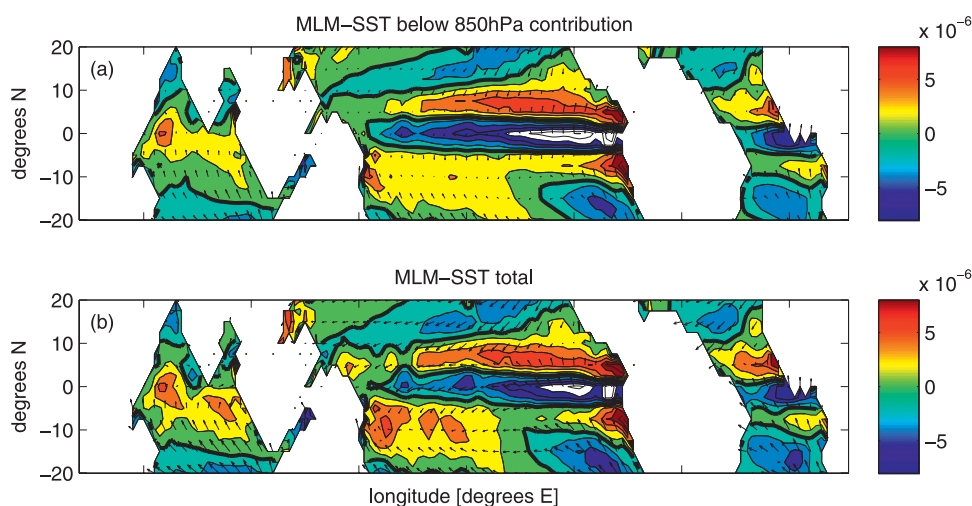


FIG. 5. MLM-SST surface winds and convergence (same plotting conventions as Fig. 2): (a) BL temperature gradient contribution only, calculated from SST and 850-hPa temperature [ $\mathbf{V}(SST, T_{850}, U_T = 0, \partial P_i = 0)$ ], and (b) the full solution [ $\mathbf{V}(SST, T_{850}, U_T, \partial P_i)$ ]. The color scale and contours are the same as Fig. 4.

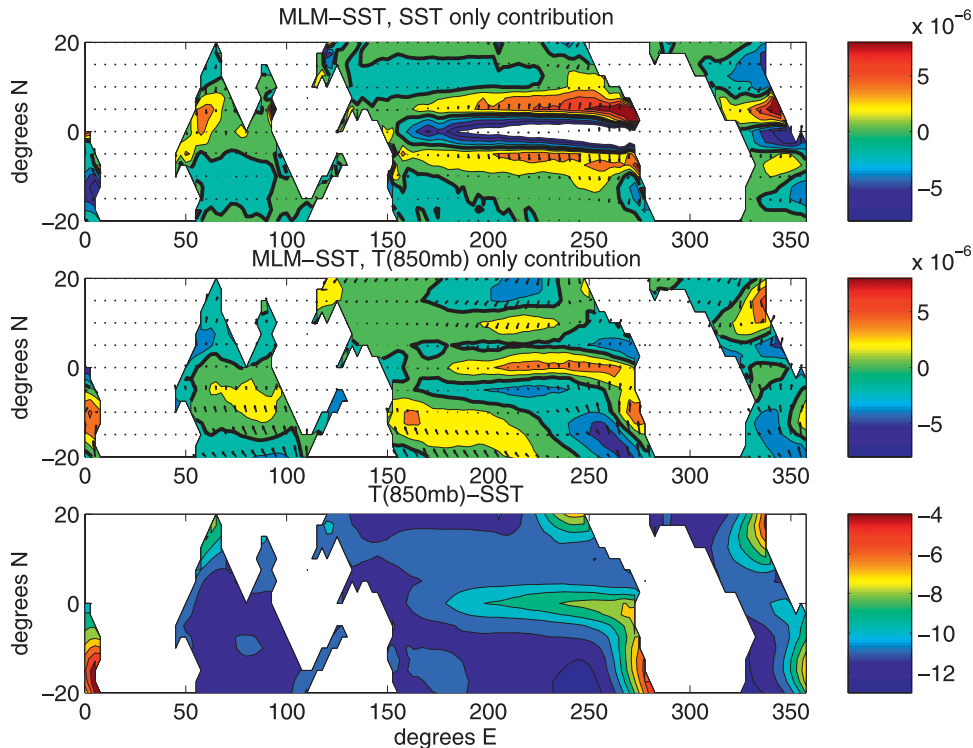


FIG. 6. Components of the MLM-SST boundary layer contribution to surface winds and convergence shown in Fig. 5a from (a) SST gradients [ $\mathbf{V}(\text{SST}, \partial T_{850} = 0, U_T = 0, \partial P_i = 0)$ ] and (b) 850-hPa horizontal temperature gradients [ $\mathbf{V}(\partial \text{SST} = 0, T_{850}, U_T = 0, \partial P_i = 0)$ ]. Here,  $1^\circ$  length arrow =  $2 \text{ m s}^{-1}$  and there are  $2 \times 10^{-6} \text{ s}^{-1}$  convergence contours. (c) The 850-hPa temperature is shown with contour spacing of 1 K.

substantial skill in reproducing the time-mean convergence field.

In the MLM-SST, the boundary layer contribution,  $\Delta P_{\text{BL}}$ , is estimated using the average of the surface and 850-hPa temperatures; therefore, this contribution can be further decomposed into a component resulting from SST and a component resulting from the 850-hPa temperature distribution. Figures 6a,b show the BL contribution to the MLM-SST separated in this manner. Although annual-mean SST and 850-hPa temperature (shown in Fig. 6c) are spatially correlated ( $r = 0.77$ ), their horizontal gradients and thus their effects on winds and convergence are rather different. Over the cold tongue, the relative uniformity of the 850-hPa temperature field reduces the boundary layer divergence implied by the SST distribution alone, and in other regions the more diffuse 850-hPa temperature maxima lead to larger regions with positive surface convergence than implied by SST alone. To the west of continents, the 850-hPa temperature field is influenced by warm advection and convection over land in addition to the nearby SSTs. The decomposition shows that although including the effects of 850-hPa temperature gradients

is important to accurately representing the climatological winds, overall BL convergence near the equator is much more strongly driven by the SST gradients than 850-hPa temperature gradients because the former are much stronger. This can be seen in the last two columns of Table 1.

Because the SST-driven component of the MLM-SST reproduces much of the observed mean-state boundary layer convergence, this model suggests that on climatological scales, boundary layer convergence is better regarded as a cause rather than a consequence of the distribution of near-equatorial deep oceanic convection. However, deep convection, along with land-ocean interactions, helps shape the patterns of convergence by affecting 850-hPa temperatures, pressure, and winds.

The MLM-SST is an incomplete analog to the LN model because 850-hPa temperature, winds, and geopotential height gradients are externally specified. In our view, these are the factors the LN back-pressure formulation stands in for. Obviously, in a closed model of surface winds, convergence, and rainfall, these fields would need to be part of the solution. One strict interpretation of the full LN model using the MLM-SST

framework would be to specify deep heating in the regions where SST drives convergence using SST only, as in Fig. 6, and then close for 850-hPa winds and pressure using something like the Gill (1980) model for the free troposphere. From Fig. 6a, it appears that this type of model would lead to an unrealistically large rainfall maximum in regions with strong SST gradients such as the eastern Pacific and too little rainfall in the western Pacific. In our companion paper, we propose that the distribution of rainfall can be better explained by including the role of conditional instability as well as the role of SST-gradient-induced boundary layer convergence in causing rainfall. In light of this idea, one potential way to close for the 850-hPa fields would be to model them using a simple Matsuno–Gill-type model for the free troposphere with specified heating over the continents and warmest SSTs.

## 5. Seasonal cycle

The boundary layer force balance at the heart of the MLM is valid on time scales much shorter than a month. Thus, it is natural to ask how much of the month-to-month and seasonal variability of surface winds and convergence is captured by this simple model.

The correlation coefficients in rows 3–6 of Table 1 summarize the seasonal and monthly skill of various previously discussed versions and parts of the MLM, compared to QuikSCAT surface vector winds and convergence from December 1999 through November 2001. These are calculated by computing monthly and seasonal [December–February (DJF), March–May (MAM), June–August (JJA), and September–November (SON)] anomalies with respect to the 2-yr time-mean state for the MLM and QuikSCAT, then computing the corresponding spatial–temporal correlation coefficient between these two fields over all months or seasons. For each month during the 2-yr period, the mean ERA-40 output for that month is used to force all versions of the MLM.

The table shows that, as for the annual mean, ERA-40 replicates the seasonal and monthly QuikSCAT wind and convergence anomalies very well. The seasonal and monthly variability in MLM-simulated convergence is also strongly correlated with observations during the time period shown ( $r = 0.82$  and  $0.65$ , respectively). As in the time mean, seasonal and monthly convergence are explained almost entirely by the MLM-BL component of the winds associated with boundary layer contributions to pressure gradients, whereas free-tropospheric winds and pressure gradients (the MLM-deep component) are more important to the surface vector wind distribution. The MLM-SST model (in which the BL

contribution to surface pressure is modeled using SST and 850-hPa temperature) is almost as skillful as the MLM in predicting seasonal and monthly surface wind anomalies but is somewhat less skillful at predicting convergence anomalies ( $r = 0.51$  and  $0.40$  for seasonal and monthly anomalies, respectively).

Figure 7 shows a typical example (for September–November) of how seasonal anomalies in QuikSCAT observations compare to the MLM and MLM-SST solutions over the tropical oceans. As in Table 1, the annual-mean winds have been subtracted to highlight the seasonal variability. In the eastern Pacific and Atlantic, shifts in the location and intensity of the ITCZ are the dominant form of seasonal variability in the QuikSCAT data and both versions of the MLM. Though substantially less skillful than the MLM (Fig. 7b), the MLM-SST (Fig. 7c) nonetheless has similar seasonal wind and convergence anomalies as the observations in most areas. As in the time-mean-state comparisons, the equatorial eastern Pacific is a particular problem area for the MLM-SST. The influence of the low-level inversion in the stratocumulus region (which is partially due to the adjacent continent) and decreased turbulent mixing over the cold tongue (which is not represented in the MLM-SST) likely account for many of the biases seen in this region.

## 6. AGCM comparison

The skill with which the simple MLM and MLM-SST models represent boundary layer convergence patterns suggests that these are quantities that are likely robustly reproduced in AGCMs forced with observed sea surface temperatures. Given the substantial variations in precipitation climatology simulated with different AGCMs, one may also ask whether intermodel differences in rainfall patterns are tied to differences in BL convergence or to other factors such as differences in the vertical structure of convection.

Figure 8 compares annual-mean  $-\omega_{850}/150$  hPa in four AGCMs forced by climatologically varying SST: the CAM3, a superparameterized version of CAM3, the GMAO NSIPP model, and the GFDL AM2 [these simulations are fully described in Wyant et al. (2006a,b)]. This measure is used as a proxy for surface convergence because the model datasets we are using unfortunately did not all include near-surface winds. The NCEP and NCEP-2 reanalyses have similar but not identical climatological relationships between surface wind convergence and 850-hPa vertical motion as in ERA-40, as estimated by linear regression between surface convergence and 850-hPa vertical motion. In NCEP (NCEP-2), a given amount of convergence at 10-m height

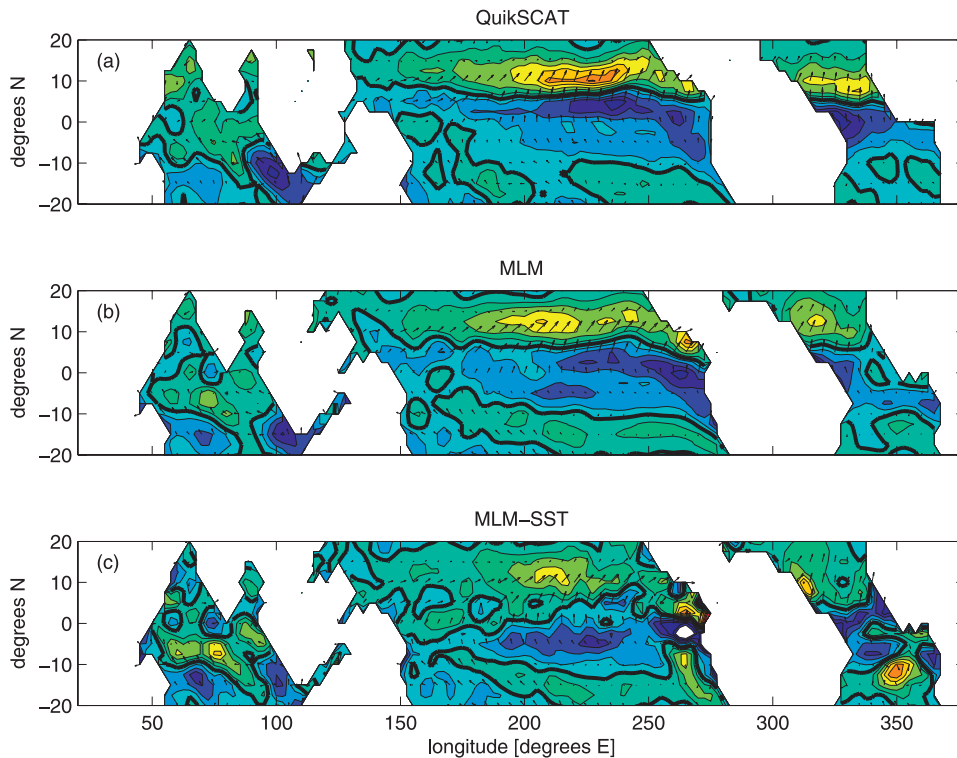


FIG. 7. SON seasonal anomalies from December 1999 to November 2001 mean surface winds and convergence for (a) QuikSCAT, (b) MLM, and (c) MLM-SST. Convergence contours are  $1 \times 10^{-6} \text{ s}^{-1}$  and  $1^\circ$  arrow =  $1 \text{ m s}^{-1}$  wind (different from previous figures).

is associated with about 30% (15%) less vertical motion than in ERA-40. This reflects slight differences between reanalyses in the vertical structure of the convergence field.

All of these GCMs have a very strong mean-state pattern correlation with the ERA-40 850-hPa vertical motion ( $r = 0.86\text{--}0.92$ ), comparable to the MLM. Intriguingly, the strength of their maximum boundary layer convergence in the central-eastern Pacific ITCZ nevertheless varies by more than a factor of 2. The standard CAM3 run has the weakest geographic variability in convergence and divergence, whereas the GMAO model has the strongest. We speculate that this again reflects model-to-model differences in the vertical structure of convergence, with the CAM3 having a very shallow layer of convergence and the GMAO model producing deep boundary layer convergence.

For comparison, Fig. 9 shows the climatological precipitation in the same simulations. Some relationship between intermodel differences in BL convergence and precipitation is visible, though the comparison is far from conclusive. In the Atlantic basin, the two simulations with stronger BL convergence (SPCAM and GMAO) also have more rainfall. Over the Indian Ocean,

the larger region of BL convergence in the CAM3 is also associated with a larger region of precipitation than in the other models. The northward extension of rainfall over the western Pacific basin in the GMAO is also seen in the BL convergence field, though not in the CAM3 climatology, which also has a northward extension of rainfall in the same region. However, in the Northern Hemisphere summer, the CAM3 boundary layer convergence extends substantially into this region, unlike in the QuikSCAT observations, the superparameterized CAM3, or the GFDL model (not shown). The GMAO simulation has the strongest correlation between mean BL convergence and precipitation.

## 7. Conclusions

The Stevens et al. (2002) mixed layer model, based on a boundary layer momentum balance between pressure-gradient forces, Coriolis acceleration, linearized friction, and downward momentum mixing, skillfully reproduces the low-latitude surface wind and convergence climatology, as well as month-to-month variability, when using as input only surface pressure and horizontal winds at the “base of the free troposphere,” here taken as 850 hPa. The linear character of this model

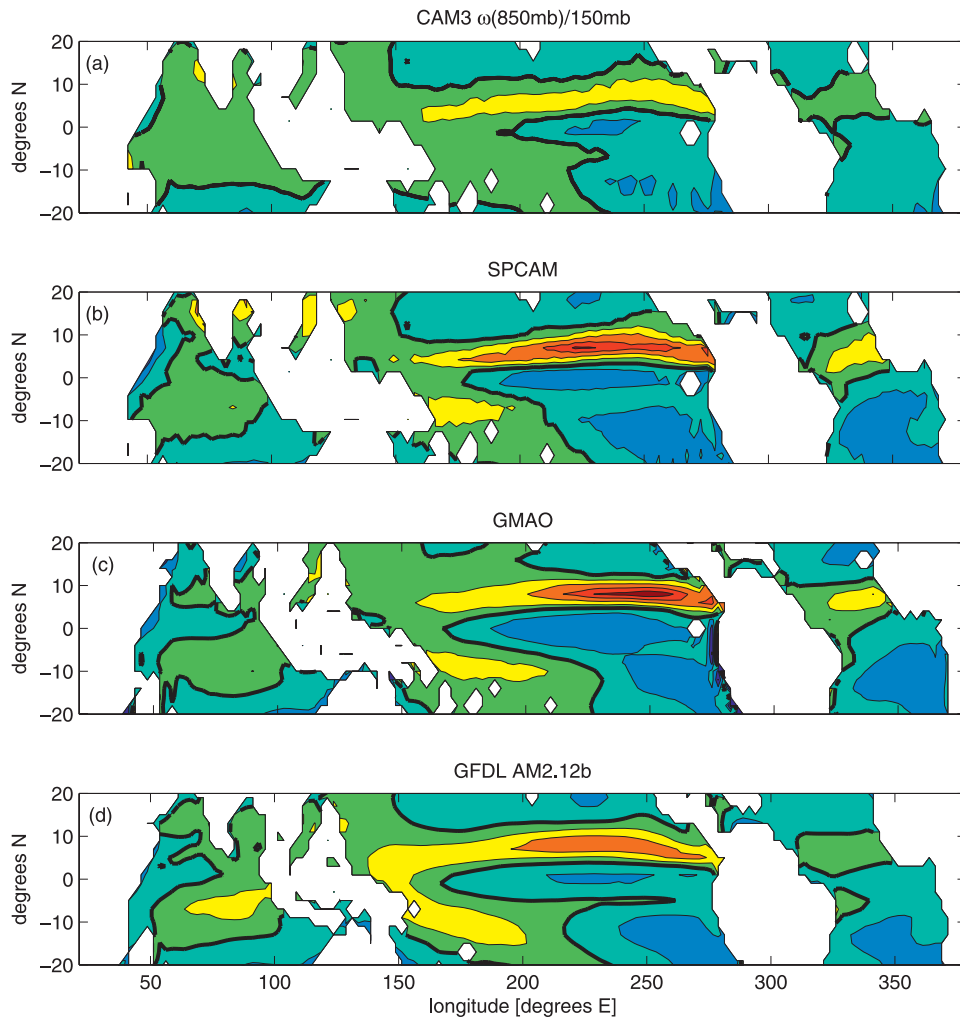


FIG. 8. Climatological  $-\omega_{850/150}$  hPa in several AGCMs ( $2 \times 10^{-6} \text{ s}^{-1}$  contours) for the (a) standard CAM3, (b) superparameterized CAM, (c) GMAO model, and (d) GFDL AM2. The color scale is the same as Fig. 1b.

allows for a straightforward separation between the pressure gradients associated with temperature gradients below the trade cumulus inversion and those associated with free-tropospheric processes. This separation shows that the observed surface zonal wind is predominantly driven by free-tropospheric pressure gradients and downward momentum mixing, in agreement with past studies. Boundary layer temperature gradients are responsible for most of the observed near-surface convergence and 850-hPa vertical motion.

To study whether climatological convergence patterns are a cause or consequence of the distribution of deep convection (when SST is specified as a boundary condition), we examined the direct contribution of SST gradients to the modeled convergence using the MLM-SST, a version of the MLM that uses SST and 850-hPa temperature to estimate the boundary layer contribu-

tion to surface winds and convergence. The MLM-SST model, though not as skillful as the MLM, predicts close to half of the geographic variance of annual-mean surface convergence, including the differences between the strong surface convergence in the Atlantic and east Pacific ITCZs and the much weaker convergence over the Indo-Pacific warm pool. Decomposing the MLM-SST boundary layer contribution into an SST component and an 850-hPa temperature component shows that, near the equator, the convergence required to support deep convection is primarily induced by SST gradients.

Although our conclusions are in broad accordance with the view proposed by LN, the MLM and MLM-SST differ in many important respects from the LN model and provide a closer analog to reality. The MLM-SST is not a closed model because the distributions of

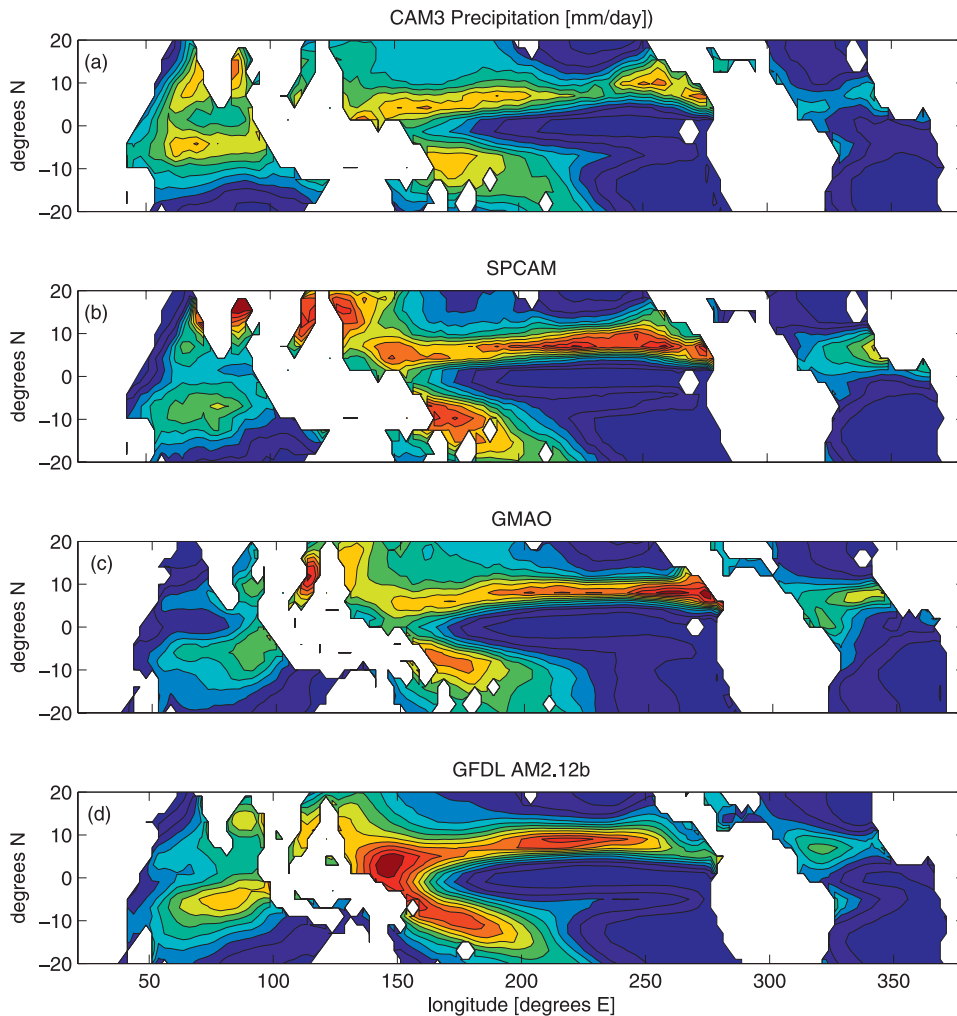


FIG. 9. Annual-mean AGCM precipitation with contours of  $1 \text{ mm day}^{-1}$ . The color scale is the same as Fig. 1c.

850-hPa horizontal winds, temperature, and geopotential height are specified. This provides the mechanism within the MLM-SST for the global distribution of convective heating to nonlocally affect convergence. This specification replaces (and thereby provides a test of) LN's back-pressure formulation for free-tropospheric feedbacks on boundary layer convergence. LN's back pressure would predict that in centers of strong SST-driven surface convergence, the free-tropospheric contribution will induce surface divergence. The MLM-SST shows that the free-tropospheric convergence contribution tends to be rather small in such regions, and in some places, such as the SPCZ, actually helps amplify the SST-driven convergence. Overall, our results do not support the LN "back-pressure feedback."

Compared to LN, the MLM and MLM-SST also use a more realistic boundary layer depth, extending to

850 hPa compared to 700 hPa in LN. In addition, LN focused on the zonally asymmetric portion of the surface winds and convergence field only, out of necessity because they neglected downward momentum mixing from above the boundary layer. The MLM and MLM-SST suffer from no such restriction.

A number of features of the precipitation distribution are not explained by boundary layer convergence alone. However, because (at least in reanalyses) surface convergence is well correlated with vertical motion at 850 hPa, our model suggests that if we can also simply predict the response of the free troposphere to the 850-hPa vertical motion distribution, we may be able to understand much of the geographical and seasonal variability we observe in rainfall and vertical motion profiles. This is the goal of our companion paper (Back and Bretherton 2009).

AGCMs forced with climatologically varying SST show similar seasonally varying patterns of 850-hPa vertical motion but with magnitudes varying twofold between models, suggesting intermodel differences in the vertical profile of boundary layer convergence. A qualitative comparison between their 850-hPa vertical motion and rainfall climatologies suggests that some, but not all, of the intermodel differences in simulated rainfall are associated with differences in boundary layer convergence magnitude, providing further motivation for our companion paper.

*Acknowledgments.* This work was supported by Grant DE-FG02-05ER63959 from the DOE ARM program and Grant NA06OAR4310055 from the NOAA CPPA program. Thanks to Matt Wyant for providing the AGCM data and Dennis Hartmann and Robert Wood for comments on an earlier version of this work. Reviewer comments as well as comments by Adam Sobel have also helped to improve this work.

#### REFERENCES

- Adler, R. F., and Coauthors, 2003: The Version-2 Global Precipitation Climatology Project (GPCP) Monthly Precipitation Analysis (1979–present). *J. Hydrometeorol.*, **4**, 1147–1167.
- Ahlgrimm, M., and D. Randall, 2006: Diagnosing monthly mean boundary layer properties from reanalysis data using a bulk boundary layer model. *J. Atmos. Sci.*, **63**, 998–1012.
- Back, L. E., and C. S. Bretherton, 2006: Geographic variability in the export of moist static energy and vertical motion profiles in the tropical Pacific. *Geophys. Res. Lett.*, **33**, L17810, doi:10.1029/2006GL026672.
- , and —, 2009: A simple model of climatological precipitation and vertical motion patterns over the tropical oceans. *J. Climate*, in press.
- Bacmeister, J. T., and M. J. Suarez, 2002: Wind stress simulations and the equatorial momentum budget in an AGCM. *J. Atmos. Sci.*, **59**, 3051–3073.
- Battisti, D. S., E. S. Sarachik, and A. C. Hirst, 1999: A consistent model for the large-scale steady surface atmospheric circulation in the tropics. *J. Climate*, **12**, 2956–2964.
- Biasutti, M., A. H. Sobel, and Y. Kushnir, 2006: AGCM precipitation biases in the tropical Atlantic. *J. Climate*, **19**, 935–958.
- Chiang, J. C. H., and S. E. Zebiak, 2000: Surface wind over tropical oceans: Diagnosis of the momentum balance, and modeling the linear friction coefficient. *J. Climate*, **13**, 1733–1747.
- , —, and M. A. Cane, 2001: Relative roles of elevated heating and surface temperature gradients in driving anomalous surface winds over tropical oceans. *J. Atmos. Sci.*, **58**, 1371–1394.
- de Szoek, S. P., C. S. Bretherton, N. A. Bond, M. F. Cronin, and B. M. Morley, 2005: EPIC 95°W observations of the eastern Pacific atmospheric boundary layer from the cold tongue to the ITCZ. *J. Atmos. Sci.*, **62**, 426–442.
- Fu, R., A. D. Genio, and W. Rossow, 1994: Influence of ocean surface conditions on atmospheric vertical thermodynamic structure and deep convection. *J. Climate*, **7**, 1092–1108.
- Gill, A. E., 1980: Some simple solutions for heat-induced tropical circulation. *Quart. J. Roy. Meteor. Soc.*, **106**, 447–462.
- Holland, J., and E. Rasmusson, 1973: Measurements of the atmospheric mass, energy, and momentum budgets over a 500-kilometer square of tropical ocean. *Mon. Wea. Rev.*, **101**, 44–57.
- Kalnay, E., and Coauthors, 1996: The NCEP/NCAR 40-Year Reanalysis Project. *Bull. Amer. Meteor. Soc.*, **77**, 437–471.
- Kanamitsu, M., W. Ebisuzaki, J. Woollen, S.-K. Yang, J. J. Hnilo, M. Fiorino, and G. L. Potter, 2002: NCEP–DOE AMIP-II reanalysis (R-2). *Bull. Amer. Meteor. Soc.*, **83**, 1631–1643.
- Kubar, T. L., D. L. Hartmann, and R. Wood, 2007: Radiative and convective driving of tropical high clouds. *J. Climate*, **20**, 5510–5526.
- Lindzen, R. S., and S. Nigam, 1987: On the role of sea surface temperature gradients in forcing low-level winds and convergence in the tropics. *J. Atmos. Sci.*, **44**, 2418–2436.
- McGauley, M., C. Zhang, and N. Bond, 2004: Large-scale characteristics of the atmospheric boundary layer in the eastern Pacific cold tongue–ITCZ region. *J. Climate*, **17**, 3907–3920.
- Mote, P. W., and R. Frey, 2006: Variability of clouds and water vapor in low latitudes: View from Moderate Resolution Imaging Spectroradiometer (MODIS). *J. Geophys. Res.*, **111**, D16101, doi:10.1029/2005JD006791.
- Neelin, J. D., 1989: On the interpretation of the Gill model. *J. Atmos. Sci.*, **46**, 2466–2468.
- Sobel, A. H., and J. D. Neelin, 2006: The boundary layer contribution to intertropical convergence zones in the quasi-equilibrium tropical circulation model framework. *Theor. Comput. Fluid Dyn.*, **20** (5–6), 323–350.
- Stevens, B., J. J. Duan, J. C. McWilliams, M. Münnich, and J. D. Neelin, 2002: Entrainment, Rayleigh friction, and boundary layer winds over the tropical Pacific. *J. Climate*, **15**, 30–44.
- Trenberth, K. E., D. P. Stepaniak, and J. M. Caron, 2000: The global monsoon as seen through the divergent atmospheric circulation. *J. Climate*, **13**, 3969–3993.
- Uppala, S. M., and Coauthors, 2005: The ERA-40 Re-Analysis. *Quart. J. Roy. Meteor. Soc.*, **131**, 2961–3012.
- Wang, B., and T. M. Li, 1993: A simple tropical atmosphere model of relevance to short-term climate variations. *J. Atmos. Sci.*, **50**, 260–284.
- Wu, Z., D. S. Battisti, and E. S. Sarachik, 2000: Rayleigh friction, Newtonian cooling, and the linear response to steady tropical heating. *J. Atmos. Sci.*, **57**, 1937–1957.
- Wyant, M. C., C. S. Bretherton, J. T. Bacmeister, J. T. Kiehl, I. M. Held, M. Zhao, S. A. Klein, and B. A. Soden, 2006a: A comparison of low-level cloud properties and their response to climate change in three AGCMs sorted into regimes using mid-tropospheric vertical velocity. *Climate Dyn.*, **27**, 261–279.
- , M. Khairoutdinov, and C. S. Bretherton, 2006b: Climate sensitivity and cloud response of a GCM with a superparameterization. *Geophys. Res. Lett.*, **33**, L06714, doi:10.1029/2005GL025464.
- Zebiak, S. E., 1982: A simple atmospheric model of relevance to El Niño. *J. Atmos. Sci.*, **39**, 2017–2027.
- , 1986: Atmospheric convergence feedback in a simple model for El Niño. *Mon. Wea. Rev.*, **114**, 1263–1271.
- Zhang, C., M. McGauley, and N. A. Bond, 2004: Shallow meridional circulation in the tropical eastern Pacific. *J. Climate*, **17**, 133–139.